

# FINITE ELEMENT COMPUTATIONS OF TWO-DIMENSIONAL ARTERIAL FLOW IN THE PRESENCE OF A TRANSVERSE MAGNETIC FIELD

G. C. SHARMA AND JAYA KAPOOR

*Department of Mathematics, Institute of Basic Science, Khandari, Agra 282002, India*

## SUMMARY

A finite element solution of the Navier–Stokes equations for steady flow under the magnetic effect through a double-branched two-dimensional section of a three-dimensional model of the canine aorta is discussed. The numerical scheme involves transforming the physical co-ordinates to a curvilinear boundary-fitted co-ordinate system. The shear stress at the wall is calculated for a Reynolds number of 1000 with the branch-to-main aortic flow rate ratio as a parameter. The results are compared with earlier works involving experimental data and found to be in reasonable qualitative agreement. The steady flow, shear stress and branch flow under the effect of a magnetic field have been discussed in detail.

KEY WORDS finite element; arterial flow; magnetic field; co-ordinate transformation

## INTRODUCTION

The measurement of shear stress in arterial flow has acquired importance because of the possible relation between the shear stress at the wall and the existence of atherosclerosis.

Flow phenomena in large and medium-sized arteries influence the development of atherosclerosis lesions. Atherosclerosis is a degenerative disease caused by the collection of lipids and other materials under the endothelial layers lining the arterial wall. These areas of collection are called plaques. The greatest possibility for the disease is in the space near bends, junctions and branches of large arteries. Fry<sup>1</sup> assumed that these plaques represent the tissue response to an increased flux of plasma substances across an endothelial surface.

Application of a magnetic field has been realized as an elegant device for flow control in physiological fluid flows. Davis and Ray<sup>2</sup> computed the flow in zero-degree bifurcation. Lutz *et al.*<sup>3</sup> considered a simplified model of a double-branched network that shows the region from the thoracic aorta and includes the celiac and mesenteric branches (Figure 1). Wei *et al.*<sup>4</sup> and Ehrlich<sup>5</sup> have considered the problem of obtaining the solution in complex geometries by applying a co-ordinate transformation technique. Singh<sup>6</sup> studied the hydromagnetic effects on the three-dimensional flow past a porous plate.

Much of the numerical work has been done using the finite element technique in biofluid mechanics. Gokhle *et al.*<sup>7</sup> used the finite element method to solve the steady state Navier–Stokes equations in a

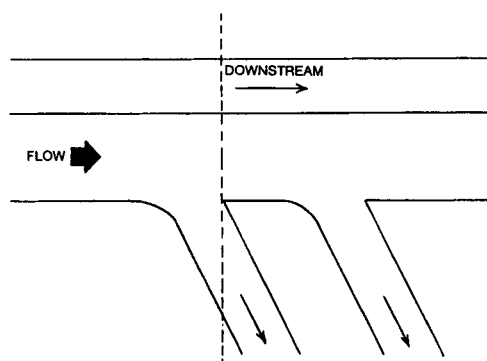


Figure 1. Aortic model geometry

two-dimensional section of the geometry considered by Lutz *et al.*<sup>3</sup> Mishra and Singh<sup>8</sup> studied the non-linear flow of blood through arteries. Thompson *et al.*<sup>9</sup> considered a numerical technique for generating a boundary-fitted co-ordinate system, which was further developed by Anderson *et al.*<sup>10</sup>

It is well known that the action at a distance of a magnetic field on a fluid has many practical applications. Examples are the control of liquid metals in continuous casting processes, plasma welding and in blood plasma. The field of MHD is complex since it involves the solution of both the Navier–Stokes equations characterizing fluid flow and Maxwell’s equations for the magnetic field. In most situations, analytic solutions of the coupled sets of equations do not exist. Numerical techniques have proved the only means available for addressing realistic physiological problems.

The purpose of this work is to investigate the fluid mechanics of steady flow for a two-dimensional finite element model under the influence of a transverse magnetic field. The fluid is chosen to be Newtonian and incompressible and the flow is assumed in the region of the arterial system. Here the numerical scheme involves first the transformation of co-ordinates and then the resulting transformation parameters are used in the weak formulation of the finite element solution of the transformed equations and boundary conditions under the effect of a magnetic field transverse to the flow.

We used the finite element technique to complete the results and the shear stress at the wall is calculated for a Reynolds number of 1000. It is found that our results are very close to the exact solutions. The numerical results are then compared with the results of Agonafer *et al.*<sup>11</sup> The magnetic field reduces the flow.

#### TRANSFORMATION OF CO-ORDINATES

The following elliptic equations are used to generate the boundary-fitted co-ordinate system:

$$\frac{\partial^2 \xi}{\partial x^2} + \frac{\partial^2 \xi}{\partial y^2} = 0, \quad (1)$$

$$\frac{\partial^2 \eta}{\partial x^2} + \frac{\partial^2 \eta}{\partial y^2} = 0. \quad (2)$$

These equations constitute a transformation from the physical plane (Figure 2) to a computational plane. Since this transformation is governed by the elliptic equations, it is called elliptic grid generation, first used on a practical basis by Thompson *et al.*<sup>9</sup> in 1974.

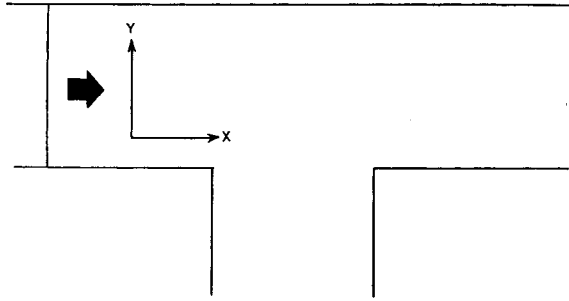


Figure 2. Single-branched geometry

Interchanging dependent and independent variables in equation (1), we have

$$\alpha \frac{\partial^2 x}{\partial \xi^2} - 2\beta \frac{\partial^2 x}{\partial \xi \partial \eta} + \gamma \frac{\partial^2 x}{\partial \eta^2} = 0, \quad (3)$$

$$\alpha \frac{\partial^2 y}{\partial \xi^2} - 2\beta \frac{\partial^2 y}{\partial \xi \partial \eta} + \gamma \frac{\partial^2 y}{\partial \eta^2} = 0, \quad (4)$$

where

$$\begin{aligned} \alpha &= \left( \frac{\partial x}{\partial \eta} \right)^2 + \left( \frac{\partial y}{\partial \eta} \right)^2, \\ \beta &= \frac{\partial x}{\partial \xi} \frac{\partial x}{\partial \eta} + \frac{\partial y}{\partial \xi} \frac{\partial y}{\partial \eta}, \\ \gamma &= \left( \frac{\partial x}{\partial \xi} \right)^2 + \left( \frac{\partial y}{\partial \xi} \right)^2. \end{aligned}$$

Here  $x$  and  $y$  are the independent variables and  $\alpha$ ,  $\beta$  and  $\gamma$  are the co-ordinate transformation parameters.

### GOVERNING FIELD EQUATIONS

In this analysis the assumptions are that the fluid is incompressible, isothermal and Newtonian and the flow is steady and laminar. To achieve the steady state solution, it is easier computationally to retain the unsteady state terms and to get the steady state solution asymptotically in time.

The conservation-of-mass and time-dependent Navier–Stokes equations in primitive variables replaced by the vorticity transport equation and the elliptic streamfunction equation in Cartesian rectangular co-ordinates are

$$\frac{\partial \omega}{\partial t} + u \frac{\partial \omega}{\partial x} + v \frac{\partial \omega}{\partial y} = \frac{1}{Re} \left( \frac{\partial^2 \omega}{\partial x^2} + \frac{\partial^2 \omega}{\partial y^2} \right) - M^2 u, \quad (5)$$

where  $M$  is the magnetic field distribution or Hartmann number.

The continuity equation can be satisfied by the introduction of the streamfunction  $\Psi$ ,

$$\frac{\partial^2 \psi}{\partial x^2} + \frac{\partial^2 \psi}{\partial y^2} = -\omega, \quad (6)$$

and we have

$$u = \frac{\partial \psi}{\partial y}, \quad (7)$$

$$v = -\frac{\partial \psi}{\partial x}. \quad (8)$$

Equations (7) and (8) imply

$$\omega = \frac{\partial v}{\partial x} - \frac{\partial u}{\partial y}. \quad (9)$$

Equation (5) can be transformed to the numerical plane  $(\xi, \eta)$ , resulting in

$$\frac{\partial \omega}{\partial t} + \frac{y_\eta(u\omega)_\xi - y_{\xi\eta}(u\omega)_\eta}{J} + \frac{x_\xi(v\omega)_\eta - x_\eta(v\omega)_\xi}{J} = \frac{(\alpha\omega_{\xi\xi} - 2\beta\omega_{\xi\eta} + \gamma\omega_{\eta\eta} + \alpha\omega_\eta + \tau\omega_\xi)}{J^2 Re} - M, \quad (10)$$

where  $Re$  is the Reynold number. We have

$$\alpha\Psi_{\xi\xi} - 2\beta\Psi_{\xi\eta} + \gamma\Psi_{\eta\eta} + \alpha\Psi_\eta + \gamma\Psi_\xi = -J^2\omega, \quad (11)$$

where

$$\alpha = -J^2p, \quad \tau = -J^2Q. \quad (12)$$

### INITIAL CONDITION

For the initial value vorticity transport equation we require the initial vorticity distribution. Since we are not interested in time-dependent solutions, a standard initial streamfunction distribution is calculated by solving the potential flow equations. By applying a no-slip condition at the solid wall boundaries, the initial vorticity distribution can be defined.

### BOUNDARY CONDITIONS

Assuming  $\psi = \text{constant}$ , i.e. no mass flux at solid boundaries, the boundary conditions at the wall can be derived from equation (11) as

$$\omega_{\text{wall}} = \begin{cases} -\gamma/J^2 & \text{along } \eta = \text{constant}, \\ -\alpha/J^2 & \text{along } \xi = \text{constant}, \end{cases}$$

$$\frac{\partial \Psi}{\partial n} = 0,$$

where  $\partial\Psi/\partial n$  is the derivative along the normal.

The streamfunction  $\Psi$  at the wall is specified from the knowledge of the flow parameter, the branch-to-main aortic flow rate ratio.

At inflow  $(\partial\Omega_a)$  a fully developed flow is assumed. The vorticity and streamfunction are then calculated from the knowledge of the vorticity distribution. Thus we have

$$\Psi = \psi(\eta), \quad \omega = \omega(\eta).$$

At outflow ( $\partial\Omega_b$ ) the derivative of the velocity component in the  $x$ -direction can be assumed to be zero. This gives

$$\begin{aligned} \omega_\eta &= 0, & \Psi_{\eta\eta} &= 0 & \text{along } \eta &= \text{constant,} \\ \omega_\xi &= 0, & \Psi_{\xi\xi} &= 0 & \text{along } \xi &= \text{constant.} \end{aligned}$$

NUMERICAL METHODS

In equation (6) we consider ( $\partial\Omega_\alpha$ ) as an essential boundary and  $\partial\Omega_{b+c_1+c_2+c_3+c_4+d}$  as a natural boundary. The weak formulation of equation (6) is

$$\int_{\Omega} -\nabla w \cdot \nabla \Psi \, d\Omega = - \int_{\Omega} w\omega \, d\Omega, \tag{13}$$

where  $w = \hat{\Psi}_k$  and  $\Psi = \hat{\Psi}_k \Psi_k$ , with  $\Psi_k$  denoting the shape function associated with  $k$ . There is no contribution from the natural boundary, since  $\partial\Psi/\partial n = 0$  there. On the grid shown in Figure 3, using bilinear elements, the vorticity  $\omega$  and streamfunction  $\Psi$  can be determined in the interior of the domain and on  $\partial\Omega_b$ . From the RHS of equation (13), given values of  $\Psi$  on  $\partial\Omega_{c_1+c_2+c_3+c_4}$  and  $\partial\Omega_d$ , the nodal equations can be obtained and  $\omega$  can be determined on these boundaries. By using a lumped  $\omega$ , equation (5) then becomes well-posed. The weak formulation of equation (9) is

$$\int_{\Omega} w \frac{\partial \omega}{\partial t} \, d\Omega + \int_{\Omega} w \bar{V} \cdot \nabla \omega \, d\Omega = \int_{\Omega} v w \nabla^2 \omega \, d\Omega - M,$$

where  $v$  is the kinematic pressure,  $w$  is a weighting function and  $\bar{V}$  is the velocity vector.

After integrating by parts and using lumping, the equation thus obtained is in the form

$$M_i \frac{\partial \omega_i}{\partial t} + \sum_j A_{ij} \omega_j = 0, \tag{14}$$

where the index  $j$  describes the neighbourhood of node  $i$ . The above equation can be integrated with a two-stage time- stepping scheme (for second-order accuracy in time):

$$M_i [\omega_i(t + \frac{1}{2}\Delta t) - \omega_i(t)] = -(\Delta t/2) \sum_j A_{ij}(t) \omega_j(t), \tag{15}$$

$$M_i [\omega_i(t + \Delta t/2) - \omega_i(t)] = -\Delta t \sum_j A_{ij}(t + \Delta t/2) \omega_j(t + \Delta t/2). \tag{16}$$



Figure 3. Numerically generated curvilinear co-ordinate lines

At each time step  $\Psi$  is estimated from equation (13), new values of  $\omega$  on solid boundaries are determined and a new velocity field is calculated from equations (7) and (8). This can be processed in a finite element as

$$\int_{\Omega} wu \, d\Omega = \int_{\Omega} w \frac{\partial \Psi}{\partial y} \, d\Omega,$$

$$\int_{\Omega} wv \, d\Omega = - \int_{\Omega} w \frac{\partial \Psi}{\partial x} \, d\Omega.$$

Lumping is essential on the LHS to remove the non-positivity of the system and to make the solution explicit.

The above process can be continued until a steady state is reached. For small values of  $\nu$ , i.e. for convection-dominated flow, the steady state corresponding to equation (14) provides oscillating solutions called 'wiggles'.

### DISCUSSION OF RESULTS

The numerical method was first tested by studying the fluid mechanics in a related geometry considered by previous investigators. The natural co-ordinate lines generated by transforming the physical co-ordinates in Figure 2 are shown in Figure 3. The fluid mechanics problem was solved using the FEM. Figures 4(a) and 4(b) show comparisons of the upstream and downstream wall vorticity distributions respectively. These comparisons are between the work of Agonafer *et al.*<sup>11</sup> and the present work. Our results are closer to the experimental results in comparison with Agonafer *et al.*<sup>11</sup> in the downstream region (Figure 4(b)), whereas in the upstream region both results show good agreement with the experimental results apart from small differences. In this investigation the central processing time required for the steady state flow was 45s on an IBM PC-AT 386 (INTEL).

Figure 5 shows the numerically generated curvilinear co-ordinate lines of Figure 1. In the present work the flow parameters assumed in the fluid mechanics are the branch-to-main flow rate ratio and the Hartmann number  $M$ . The calculated ventral shear rates in the celiac branch for three different flow rate ratios in the presence of magnetic field ( $M=100$ ) are shown in Figure 6. Comparison with the shear rate in the absence of the magnetic field indicates that the magnetic field is not favourable to the flow. In all three cases the curves have same lines with shear rate values at the entrance and exit for fully

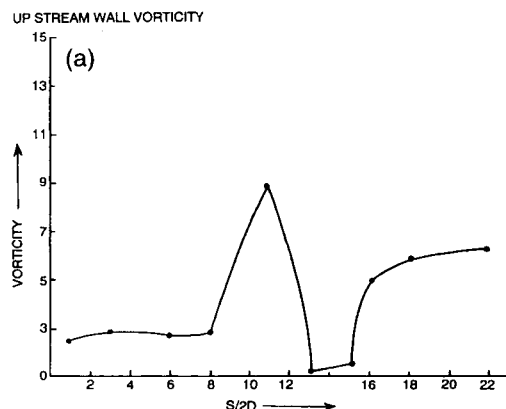


Figure 4(a). Wall vorticity distribution

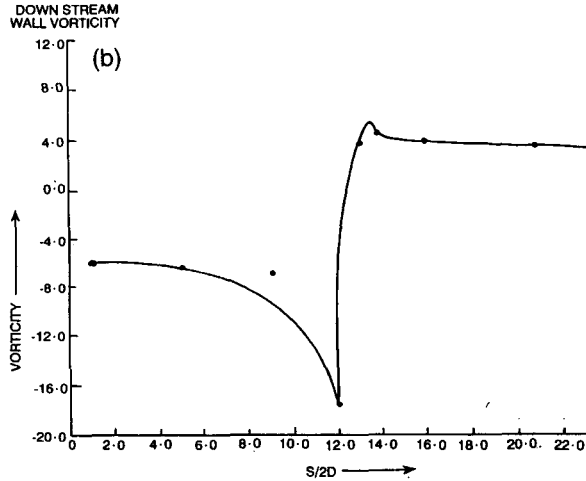


Figure 4(b). Wall vorticity distribution

developed flow, but, as shown, the shear rate values reach a local maximum at one point and quickly drop to zero or negative values before increasing at the exit point. This is also true physically, because the shear rate is maximum before bifurcation takes place, while at the bifurcation junction, since the stream is divided into two, the shear rate drops suddenly. The same thing happens when the next bifurcation takes place.

Figure 7 shows the experimental shear rates corresponding to Figure 6. The numerical shear rates are seen to compare quite well with the experimental results. The main difference between Figures 6 and 7 is that the numerical calculations, in sharp contrast with the experimental results, exhibit a flow separation phenomenon and this becomes significant in the presence of a magnetic field.

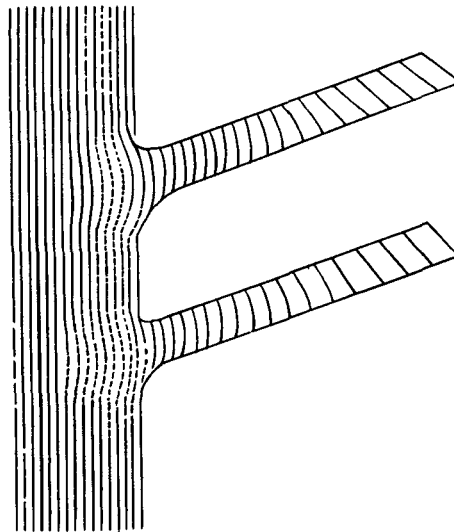


Figure 5. Numerically generated curvilinear co-ordinate lines

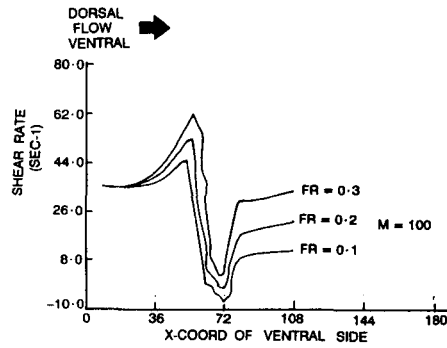


Figure 6. Numerical shear rate distribution

Experimental and numerical velocity vectors are compared in Figures 8 and 9 respectively for a branch flow rate of 20 per cent and  $M=100$ . In conclusion, the numerical calculations of steady flow in the two-dimension model of the canine aorta in the presence of a magnetic field are quite similar to the experimental results. The finite element method provides a good alternative to other methods for studying such complex biological flow geometries. The effect of the magnetic field is an efficient device for flow control. Other effects such as the pulsatile flow of elastic walls can also be incorporated into the basic approach.

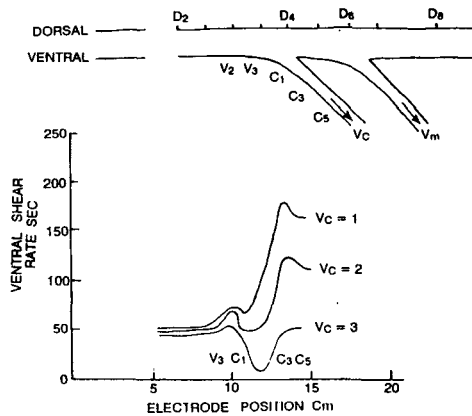


Figure 7. Experimental shear rate distribution

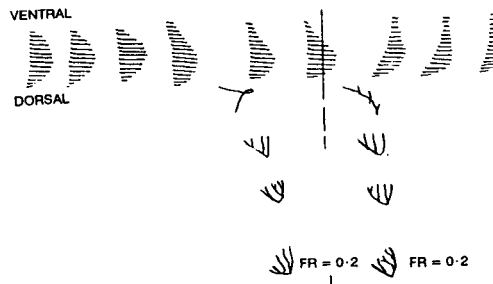


Figure 8. Numerical steady flow velocity profiles

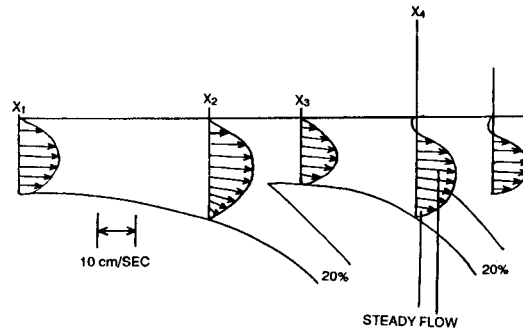


Figure 9. Experimental steady flow velocity profiles.

#### ACKNOWLEDGEMENTS

The authors are grateful to the learned referee for his valuable comments. This research has been supported by UGC grant F 8-20/91.

#### REFERENCES

1. D. L. Fry, *Circulat. Res.*, **24**, 93-108 (1969).
2. N. Davs and G. Ray, *Penn State Univ. Eng. Res. Bull.*, **B-102**, 1-54 (1971).
3. R. J. Lutz, L. Hsu, A. Menawat, J. Zrubek and K. Edwards, *74th Ann. AIChE Meet.*, New Orleans, LA, 1981.
4. B. D. Wei, L. C. Cheng, M. E. Clark and J. M. Robertson, *Proc. 33rd Ann. Conf. of Medicine and Biology*, Washington, DC, p. 110.
5. L. W. Erhlich, *J. Biomech.*, **10**, 623-631 (1977).
6. K. D. Singh, *J. Appl. Math. Phys.*, **41**, 441-447 (1990).
7. V. V. Gokhle, R. I. Tanner and K. B. Bischoff, *J. Biomech.*, **11**, 241-249 (1978).
8. J. C. Mishra and S. I. Singh, *Bull. Math. Biol.*, **49**, 257-277 (1987).
9. J. F. Thompson, F. C. Thomas and C. W. Mastin, *J. Comput. Phys.*, **15**, 299-319 (1974).
10. J. D. Anderson, G. Degrez and E. Dick, *Computational Fluid Dynamics*, Berlin, 1992.
11. D. Agonafer, C. B. Watkins and J. N. Cannon, *J. Biomech.*, **18**, 695-701 (1985).